




Exact dispersion relation of the quantum Langmuir waveTian-Xing Hu ¹, Dong Wu ^{1,*}, Z. M. Sheng ² and J. Zhang^{1,3,†}¹*Key Laboratory for Laser Plasmas and School of Physics and Astronomy, and Collaborative Innovation Center of IFSA, Shanghai Jiao Tong University, Shanghai 200240, China*²*Institute for Fusion Theory and Simulation, Department of Physics, Zhejiang University, Hangzhou 310027, China*³*Institute of Physics, Chinese Academy of Sciences, Beijing 100190, China*

(Received 23 January 2024; accepted 10 June 2024; published 24 June 2024)

The normal modes, i.e., the eigensolutions to the dispersion relation equation, are the most fundamental properties of a plasma. The real part indicates the intrinsic oscillation frequency while the imaginary part the Landau damping rate. In most of the literature, the normal modes of quantum plasmas are obtained by means of small damping approximation, which is invalid for high- k modes. In this paper, we solve the exact dispersion relations via the analytical continuation scheme, and, due to the multi-value nature of the Fermi-Dirac distribution, reformation of the complex Riemann surface is required. It is found that the topological shape of the root locus in quantum plasmas is quite different from classical ones, in which both real and imaginary frequencies of high- k modes increase with k steeper than the typical linear behavior in classical plasmas. As a result, the time-evolving behavior of a high- k initial perturbation becomes ballistic-like in quantum plasmas.

DOI: [10.1103/PhysRevE.109.065213](https://doi.org/10.1103/PhysRevE.109.065213)**I. INTRODUCTION**

The study of quantum plasmas has important applications in the fields of, e.g., astrophysics [1], nanophysics [2,3], warm dense matter [4], and inertial confinement fusion [5–8], and thus received widespread attention in recent years. However, some of its fundamental properties have rarely been seriously discussed. For example, the exact eigensolution of a degenerate quantum plasma. In this paper, we solve the Landau damping rate by means of analytical continuation (AC) method, and avoid the branch cut discontinuity by extending the Riemann surface of the one-dimensional Fermi-Dirac distribution function (1DFDDF). The AC method is a crucial step to comprehend the damping normal modes of plasmas, proposed by Landau a long time ago [9,10], which is widely used in the field of classical plasmas, but rarely discussed for quantum plasmas. The AC method is able to solve the exact dispersion relation of normal modes (in our case, the Langmuir wave) with arbitrarily high wave numbers, which are important when microscale quantum kinetic effects are involved.

The electrons in metals or semiconductors are the most common and well-known example of quantum plasma. However, the behavior of electrons in such condensed matter systems are often very complex due to lattice structures of the ions and strong correlations among electrons. In this paper, we consider extremely dense quantum plasmas, in which the electron correlations are so weak that the random phase approximation [11] (RPA) can be appropriately adopted. Such a dense, degenerate electron environment is ubiquitous in

the universe. For example, the electrons in the core of main sequence stars are partially degenerate, and fully degenerate in a white dwarf. On earth, some inertial confinement fusion experiments also produce degenerate quantum plasmas, such as the fast ignition [6,12] and the double-cone ignition [5] schemes. In addition, some of the energetic cosmic rays are assumed to be related to waves and instabilities of dense plasmas [13,14]. In the aforementioned physical environments, high- k quantum kinetic effects may have a significant impact on microscale physics.

In most literature, the dispersion relation is often obtained using the small damping approximation (SDA), which is only valid for small wave numbers at which the damping rate is very small (about two orders smaller than the frequency). Solving the exact dispersion relation of quantum plasmas, on one hand, can yield the exact frequencies and lifetimes of the intrinsic mode; on the other hand, it also enables quantitative analysis of some nonlinear processes. A typical example of a nonlinear process would be three-wave interaction. Specifically, in order to obtain the energy-momentum matching condition of a three-wave interaction: $\omega_1 = \omega_2 + \omega_3$, $k_1 = k_2 + k_3$, the exact dispersion relation $\omega(k)$ of each wave is required. An important three-wave process such as parametric decay [15], two-plasmon decay [16–18], and stimulated Raman scattering [19,20], are all related to at least one Langmuir wave. Therefore, it is essential to obtain the exact dispersion relation for the whole k region of our interest.

The theoretical basis of this paper is the so-called collisionless quantum kinetic theory (QKT), which is, mathematically speaking, a Wigner-Poisson system (WPS) of equations.

The RPA scheme is actually equivalent to the linearized WPS [21]. In this paper, nonlinear effects will not be considered, and the ions are treated as an immobile background (namely, we adopt the jellium model [22]). The main

*Contact author: dwu.phys@sjtu.edu.cn†Contact author: jzhang1@sjtu.edu.cn

objective is to solve the exact dispersion relation of the quantum Langmuir wave. Meanwhile, some interesting properties of the complex quantum dielectric function will be discussed.

This paper is organized as follow. In Sec. II, we introduce the complex structure of the Fermi-Dirac distribution function, then briefly review the collisionless QKT and the corresponding linear response theory, which is the theoretical basis of this paper. In Sec. III, we discuss the complex structure of the dielectric function of quantum plasmas. And thus the exact linear dispersion relation of quantum Langmuir wave is solved by means of the aforementioned methods. Numerical simulations are also presented to verify the results. Further discussion and main conclusion are presented in Sec. IV.

II. THEORIES AND METHODS

We define a quantum parameter

$$\hat{h} \equiv \frac{\hbar\omega_p}{2E_F}, \quad (1)$$

sometime is referred to as the normalized Planck's constant. Here, $\omega_p = \sqrt{4\pi e^2 n/m_e}$ is the plasma frequency, and the Fermi energy $E_F = \hbar^2(3\pi^2 n)^{2/3}/2m_e$. It seems strange that \hat{h} is proportional to $n^{-1/2}$, since we expect that quantum effects should be stronger for higher density. However, quantum effects are also stronger for lower temperature, while \hat{h} is solely dependent on n . Hence, to measure the importance of quantum wave effects, a more appropriate choice would be

$$\tilde{h} \equiv \frac{\hbar\omega_p}{2k_B T}, \quad (2)$$

and once the degeneracy $\Theta = k_B T/E_F$ (the inverse of which measures the importance degeneracy) is fixed, decreasing \hat{h} means increasing \tilde{h} .

In this paper, we adopt the natural unit system, where $\hbar = m_e = e = k_B = 1$. And the frequency, number density, velocity, length, and energy, are normalized to ω_p , n_e (electron density), v_F (Fermi velocity), $\lambda_F = v_F/\omega_p$, and E_F respectively.

A. Analytical structure of the 1DFDDF

The equilibrium state of electron obeys the 3D Fermi-Dirac distribution (3DFDDF)

$$f_{3d}(\mathbf{v}) = \frac{3}{4\pi} \frac{1}{e^{(v^2-\mu)/\Theta} + 1}, \quad (3)$$

where the value of the chemical potential $\mu = \mu(\Theta)$ is chosen such that $\int f_{3d}(\mathbf{v}) d^3v = 1$.

As a fundamental study, we only consider the interaction of electrons to a plane wave field, hence we can integrate over the dimensions perpendicular to the wave, namely, we only care the about the 1D Fermi-Dirac distribution (1DFDDF) $f_{1d}(v_{\parallel}) = \int dv_{\perp} 2\pi v_{\perp} f_{3d}(v_{\parallel}, v_{\perp})$. It is easy to prove that (see the Appendix),

$$f_{1d}(v) = \frac{3}{4}\Theta \ln \left[e^{(\mu-v^2)/\Theta} + 1 \right]. \quad (4)$$

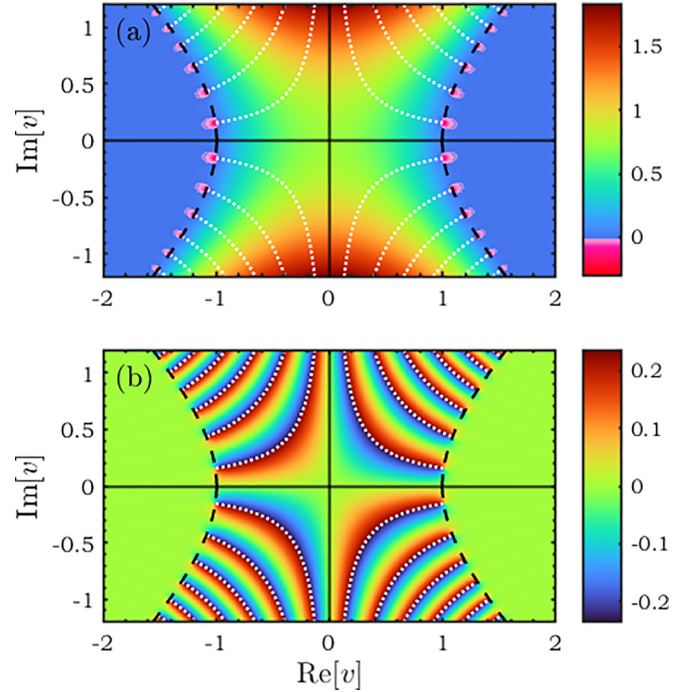


FIG. 1. (a) Real (b) Imaginary part of the 1DFDDF ($\Theta = 0.1$). The dashed lines are the hyperbolae of Eq. (6), and the white dotted lines are the branch cuts of Eq. (5).

Let v be a complex variant $v = v_r + iv_i$, then the 1DFDDF is a multivalued function, the branch cuts of which are

$$v_r v_i = \pm \frac{\pi}{2} \ell \Theta, \quad \ell \in 2\mathbb{Z}, \quad (5)$$

and the branch points are located at the hyperbola:

$$v_r^2 - v_i^2 = \mu. \quad (6)$$

The structure of the 1DFDDF is also thoroughly discussed in Ref. [23]. The density of the branch points on the hyperbola increases with decreasing Θ . In Fig. 1, we plotted the 1DFDDF in complex- v plane, one can see that its imaginary part is discontinuous at the branch cuts. These discontinuities are equal to the height of a Riemann leaf, which is $3\pi\Theta/2$ here, and they exist because we considered only a single leaf the Riemann surface, see Fig. 2(a). We refer to the 1DFDDF with an imaginary part of the form as in Fig. 2(a) as the “non-extended” 1DFDDF. However, the logarithmic multivalued analytic function has infinite leaves of Riemann surface. Figure 2(b) presented seven leaves of them. From these seven leaves, we extract out a surface that is continuous across the branch cuts, see Fig. 2(c). The 1DFDDF with an imaginary part of the form as in Fig. 2(c) is referred to as the “extended” 1DFDDF. Noticing that, after this operation, the discontinuities do not vanish, but are moved from the branch cuts to the hyperbola.

B. The Linearized WPS

The electrons in a collisionless quantum plasma obey the Wigner equation [21]

$$\partial_t f + \mathbf{v} \cdot \partial_{\mathbf{x}} f + i v \partial_{\hbar \partial_p} [\phi(\mathbf{x})] f = 0. \quad (7)$$

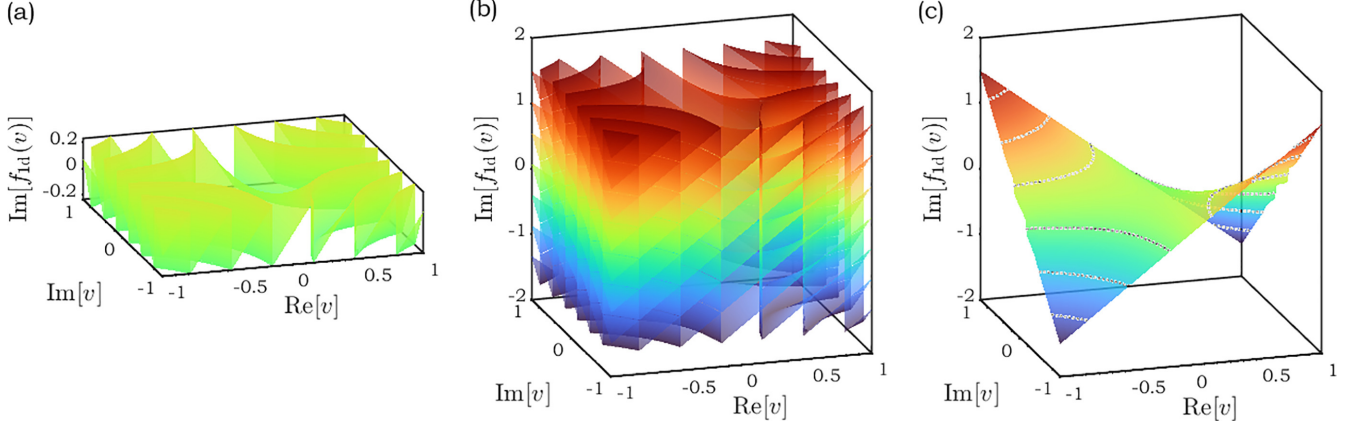


FIG. 2. (a) A single leaf (b) Seven leaves (c) Extended single leaf of the 1DFDDF ($\Theta = 0.1$) Riemann surface.

Here $f = f(\mathbf{x}, \mathbf{v}, t)$ is the Wigner quasidistribution function, which is the quantum counter part of the classical distribution function, and the pseudodifferential operator ϑ is defined by

$$\vartheta_y[O(\mathbf{x})] \equiv O\left(\mathbf{x} + \frac{\mathbf{y}}{2}\right) - O\left(\mathbf{x} - \frac{\mathbf{y}}{2}\right). \quad (8)$$

Noticing that when $y \ll x$, $\vartheta_y[O(\mathbf{x})] \simeq \mathbf{y} \cdot \nabla O$, then Eq. (7) reduces to the Vlasov equation, thus the Wigner equation is also called the quantum Vlasov equation.

And we need the Poisson equation

$$-\nabla^2 \phi = n_b - e \int f d\mathbf{v}, \quad (9)$$

where n_b stands for the background ion density, to close the system. Let $f = f_0 + \delta f$, $\phi = \phi_0 + \delta \phi$, and consider only the direction parallel to the wave vector, the linear evolution of the perturbed field can be formally written as [24]

$$\delta \phi(t, k) = \frac{i}{k^2} \iint d v_{\parallel} \frac{d \omega}{2\pi} \frac{\delta f_{k0}(v_{\parallel}) e^{-i\omega t}}{(\omega - k v_{\parallel}) \epsilon(\omega, k)}, \quad (10)$$

where $\delta f_{k0}(v)$ is the initial perturbation, and the dielectric function (DF) is defined as

$$\epsilon(\omega, k) = 1 + \frac{1}{k^2} \mathcal{W}(\hat{\hbar}\omega, \hat{\hbar}k), \quad (11)$$

where

$$\mathcal{W}(\omega, k) = \int d v \frac{\vartheta_k[f(v)]}{\omega - k v} \quad (12)$$

is the Lindhard response function [25]. As $\Theta \rightarrow \infty$, $f(v)$ tends to the Maxwellian, namely, in the classical limit, it reduces to

$$\mathcal{W}(\omega, k) = \frac{2}{\Theta} \frac{1}{\sqrt{2\pi}} \int d v \frac{v e^{-\frac{v^2}{2}}}{v - \omega/k_{\Theta}} = -\frac{2}{\Theta} Z'\left(\frac{\omega}{k_{\Theta}}\right), \quad (13)$$

where $k_{\Theta} = k\sqrt{\Theta/2}$, and Z is the famous plasma dispersion function. It is evident that in quantum plasma, the linear response function is dependent on both ω and k , but in classical plasma, it depends only on the ratio of ω to k . The response function then does not depend on $\hat{\hbar}$, which means that when Θ is large enough, the system naturally returns to classical, no matter the value of $\hat{\hbar}$.

The roots of the eigenequation

$$\epsilon(\omega, k) = 0 \quad (14)$$

yield the dispersion relation of the normal modes. Here, $\omega = \omega_r + i\omega_i$ is a complex number. To calculate the DF (11) exactly with negative value of ω_i and solve Eq. (14), AC is needed for $\omega_r = 0$ is a branch cut, namely, when $\omega_i < 0$, the response function (12) should be modified to

$$\mathcal{W}(\omega, k) = \int d v \frac{\vartheta_k[f(v)]}{\omega - k v} - 2\pi i \vartheta_k\left[f\left(\frac{\omega}{k}\right)\right], \quad (15)$$

where the $2\pi i$ term stems from the residue of the integrand of Eq. (12). In the classical limit, it is

$$\frac{\Theta}{2} \mathcal{W}(\eta) = 1 - \sqrt{2}\eta F\left(\frac{\eta}{\sqrt{2}}\right) + i\sqrt{\frac{\pi}{2}}\eta e^{-\frac{\eta^2}{2}}, \quad (16)$$

where $\eta = \omega/k_{\Theta}$, and

$$F(x) = e^{-x^2} \int_0^x e^{t^2} dt \quad (17)$$

is the Dawson integral.

III. QUANTUM LANGMUIR WAVE

A. Analytical structure of the quantum dielectric function

The Landau damping rate is the negative imaginary part of the eigenfrequency. To calculate the DF with negative imaginary frequency, analytical continuation is needed. Notice that for extremely degenerate plasmas, analytical continuation is not needed when $k < k_F = v_F = \omega_p \lambda_F^{-1}$, since the dielectric function has an analytic solution when $\Theta \rightarrow 0$:

$$\epsilon_r(\omega, k) = 1 + \frac{3}{2k^2} \left[1 + \frac{1}{2\hat{\hbar}k} (1 - b_-^2) \ln \left| \frac{1 + b_-}{1 - b_-} \right| - \frac{1}{2\hat{\hbar}k} (1 - b_+^2) \ln \left| \frac{1 + b_+}{1 - b_+} \right| \right], \quad (18)$$

$$\epsilon_i(\omega, k) = \frac{3\pi^2}{4\hat{\hbar}k^3} \ln \frac{1 + \exp[(b_+^2 - \mu)/\Theta]}{1 + \exp[(b_-^2 - \mu)/\Theta]}, \quad (19)$$

where $\epsilon = \epsilon_r + i\epsilon_i$, and

$$b_{\pm} = \frac{\omega}{k} \pm \frac{\hat{\hbar}k}{2}. \quad (20)$$

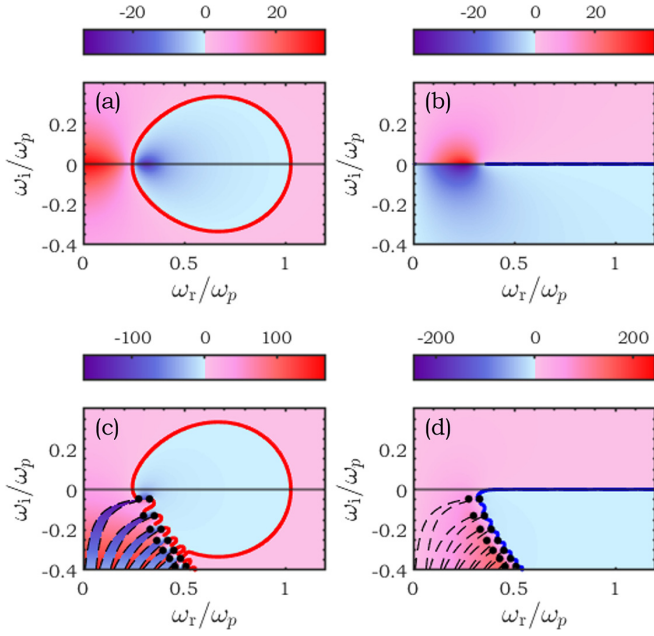


FIG. 3. [(a),(b)] Real and imaginary part of the dispersion function without analytical continuation, and (c), (d): with analytical continuation. The dashed lines are mappings of the branch cuts. The red lines stand for $\text{Re}[\epsilon(\omega, k)] = 0$, and blue lines for $\text{Im}[\epsilon(\omega, k)] = 0$.

Thus one can see than only when $|b_{\pm}| > 1$, namely,

$$-k \pm \frac{\hat{\hbar}k^2}{2} < \omega < k \pm \frac{\hat{\hbar}k^2}{2}, \quad (21)$$

the DF has finite imaginary part. The area enclosed by (21) is referred as to the electron-hole excitation continuum (EHEC), in which a plasmon delay into an electron and a hole. The

above formula is obtained based on the SDA:

$$\lim_{y \rightarrow 0} \frac{1}{x \pm iy} = \mathcal{P} \frac{1}{x} \mp i\pi\delta(x), \quad (22)$$

which is incorrect when ω_i is finite. In the following, we directly solve the Eq. (15) without any approximation scheme.

In Fig. 3, the numerical results of dispersion function with or without AC are presented ($\Theta = 0.1$, $\hat{\hbar} = 0.6$), where the wave number $k = 0.3$. The upper two panels (a) and (b) are the real and imaginary parts of the DF without AC, while the lower two are with AC. It is shown that the discontinuity of the 1DFDDF is explicitly mapped from the complex v plane to the complex ω plane by the ϑ operator, since in the calculation, we used the non-extended 1DFDDF, i.e., the single leaf Riemann surface of Fig. 2(a). The series of pairs of black dots in the lower half plane are located at two hyperbolas, whose vertices are $\mu k \pm \hat{\hbar}k^2/2$, respectively.

In the rest of this paper, the imaginary part of the DF would not be presented, but we still keep the $\text{Im}[\epsilon(\omega, k)] = 0$ lines in the real DF diagrams. And the color bar will also be neglected since the absolute values of the DF are irrelevant in the context.

Take an example of a degenerate plasma, say, with density $n = 3 \times 10^{26} \text{ cm}^{-3}$, and temperature $T = 300 \text{ eV}$. Then we have the quantum parameter $\hat{\hbar} = 0.2$ and $\Theta = 0.2$. The real DF of such parameters in complex frequency plane are plotted In Fig. 4, where the real root loci are indicated by red lines and the imaginary loci by blue lines. Noticing that the real and imaginary loci have multiple intersections, which stand for multiple solutions of the normal modes. Generally, we only care about the least damping mode, i.e., the intersection point with maximum ω_i , which we indicated by black crosses in Fig. 4 and labeled its value. In Figs. 4(a)–4(e), we used the single leaf 1DFDDF, the discontinuities occur at the branch cuts. One can see that there are no intersections in Fig. 4(e), so we have to use the extended 1DFDDF to move the

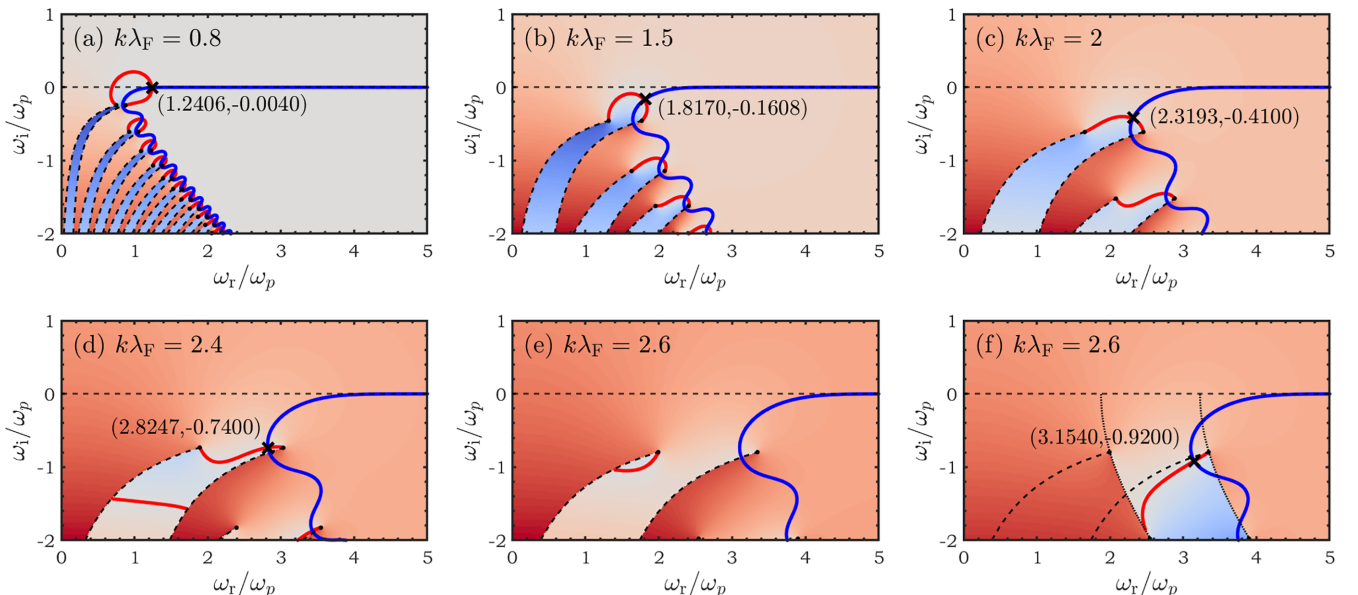


FIG. 4. Complex frequency plane of dispersion function, with $\Theta = 0.2$, $\hat{\hbar} = 0.2$.

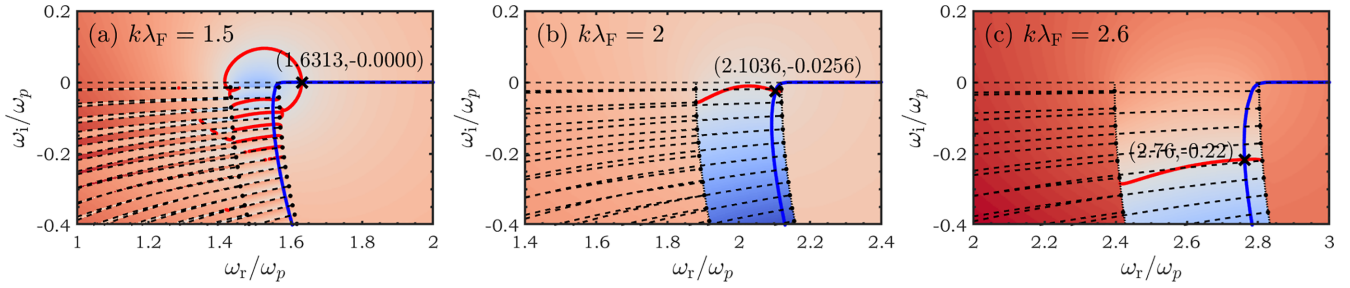


FIG. 5. Complex frequency plane of dispersion function, with $\Theta = 0.006$, $\hat{h} = 0.06$.

discontinuities to the hyperbolas, as is seen in Fig. 4(f), in which a damping mode is obtained.

For another example of extremely degenerate plasma, we choose density $n = 3 \times 10^{29} \text{ cm}^{-3}$, and temperature $T = 10^3 \text{ eV}$, which could be the interior of a typical small white dwarf. Then we have the $\hat{h} = 0.06$ and $\Theta = 0.005$. The DF results are presented in Fig. 5. One finds that, at such small Θ , the distance among each branch cuts are extremely small. All the modes with finite damping rate are located between the two hyperbolas (a gap opened by quantum wave effect). Hence the extend 1DFDDF is indispensable in this case. From Fig. 5, one also finds that when ω_i is finite,

$$\omega_r \simeq \mu k + \frac{\hat{h}k^2}{2}, \quad (23)$$

and since $\mu \rightarrow 1$ when $\Theta \rightarrow 0$, this is upper bound of the EHEC.

Now we briefly discuss the topological features of the root loci. Generally, the imaginary locus starting from $\infty + 0i$, passing through every pair of branch point, while the real locus start from one of the branch points and end with another. If the starting and ending points are a pair, and the locus is above the line joining the two branch points, we refer to this topological shape as ‘‘classical’’, for it is topologically identical to the classical solution, see Fig. 6 (The classical thumblike figure is very common in the field of classical plasma instabilities, e.g., see Ref. [26]). Otherwise it is a ‘‘quantum’’ shape. For example, the (a)–(d) panels in Fig. 4 are classical, while (d)–(f) are quantum. And in an extremely degenerate case like Fig. 5, the classical shape does not exist at all. Furthermore, a quantum shape means that the least damping mode is most likely located within the two hyperbolas.

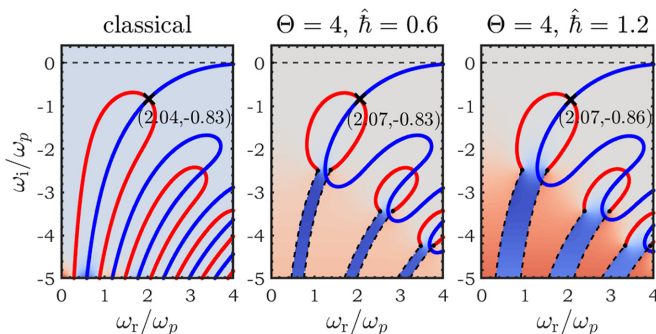


FIG. 6. The DF complex frequency plane of classical and almost-classical plasmas.

In Fig. 6, the classical sub-figure is calculated via Eq. (16), and the other two are quantum results with $\Theta = 4$, which is almost Maxwellian, it is shown that the normal modes in these three sub-figure are fairly close to one another. As $\Theta \rightarrow \infty$, all the branch points going to $-i\infty$, and we know that the value of \hat{h} (or \tilde{h}) only effects the distance between a pair of branch points. This diagrammatically demonstrated that the larger Θ is, the less important the value of \hat{h} (or \tilde{h}) is.

B. Exact solution of the normal modes

It is worth mentioning that, $\epsilon(\omega, k) = 0$ has multiple roots in a finite region of the complex ω plane, as one can see from Fig. 3, but we only care about the lowest damping mode. Hence, to solve the full dispersion relation of the QLW, we can start from $k \simeq 0^+$, and calculate a small region centered at $\omega_0 = 1 + 0^+i$ to find the first root ω_1 and record the difference $\Delta\omega_1 = \omega_1 - \omega_0$. Then we increase k with a small value and calculate a next region centered at $\omega_1 + \Delta\omega_1$ to find the second root. Repeating this procedure, then a continuous curve of the complex frequency of the QLW as a function of k is obtained. The full solutions of normal modes $\omega(k)$ with different densities are plotted in Fig. 7. In Fig. 7(a), where $\hat{h} = 0.4$ is corresponding to electron number density $n = 4 \times 10^{24} \text{ cm}^{-3}$, and $\Theta = 0.2, 0.4$, and 0.8 , are corresponding to the temperature $T = 19, 37$, and 74 eV . In Fig. 7(b), where $\hat{h} = 0.2$ corresponds to electron number density $n = 3 \times 10^{26} \text{ cm}^{-3}$, and $\Theta = 0.1, 0.2$, and 0.4 , correspond to the temperature $T = 170, 340$, and 680 eV . In Fig. 7(c), all the curves are calculated with $\Theta = 0.02$, since the shape of the curves hardly change when Θ further decreases, we annotated them as $\Theta < 0.02$, or, one can simply treat them as zero-temperature results. The dashed lines attached to each solid line are the corresponding upper bounds of the EHEC. One can see that the solid lines are slightly lower than the dashed lines only in a very small region, which means that the EHEC predicted by Eq. (21) is incorrect when k is large. This is because the derivation of Eq. (21) is based on the SDA, which is incorrect for finite damping rate.

C. Numerical benchmark of the normal modes

The WPS, i.e., Eqs. (7) and (9), can be solved numerically [27–29] as a initial value problem. We thus perform a 1D1V simulation of the WPS, i.e., we consider only one dimension in both real space and velocity space (a 2D phase space). In the simulation, we set the initial perturbation as

$$f(x, v, 0) = [1 + A \cos(k_0 x)] f_{1d}(v), \quad (24)$$

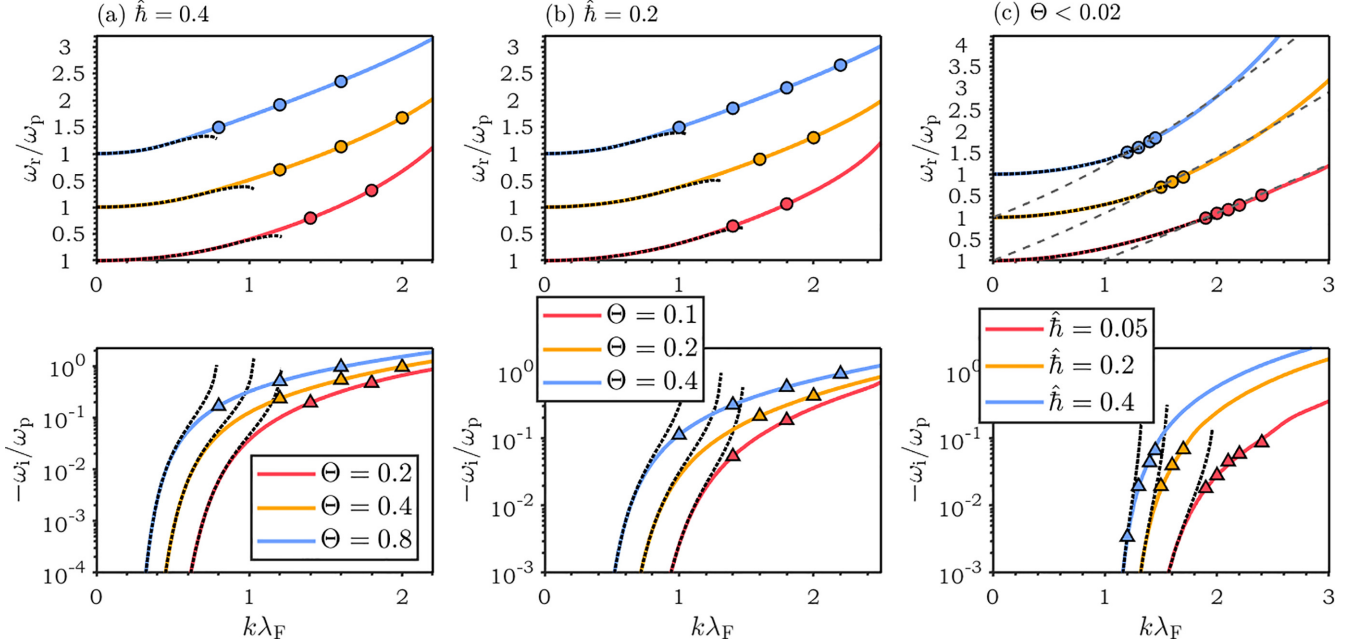


FIG. 7. Dispersion relations calculated via the SDA and AC method. Solid lines: AC results. Dotted lines: SDA results. Circled/triangular markers: frequencies/damping rates measured from Wigner-Poisson simulations. Dashed lines in (c): the damping-undamping boundary from Eq. (21).

and let it evolve, then measure the frequency and damping rate of the perturbation. The factor A is chosen to be very small to avoid nonlinear effects. When the initial perturbation is set, the time-dependent behavior of the perturbed field $\delta\phi$ consists of a ballistic mode and an infinite number of normal modes, and this can be shown by rewriting Eq. (10) as

$$\delta\phi(t, k) = \frac{1}{k^2} \int dv \delta f_{k0}(v) \times \left[\frac{e^{-ikvt}}{\epsilon(kv, k)} + \sum_n \frac{e^{-i\omega_n t}}{(\omega_n - kv)\partial_{\omega_n}\epsilon} \right], \quad (25)$$

where the first term in the bracket stands for the ballistic mode while the second is the normal modes.

Some results are presented also in Fig. 7, where the colored circles stand for real frequency measured from simulation result, and the triangles for damping rate. In addition, there is a dotted line attached to each colored line, which is calculated by SDA scheme, where the real part of the frequency ω_r is the root of the equation

$$\epsilon_r = 1 + \frac{3}{2k^3} [g(b_+) - g(b_-)] = 0. \quad (26)$$

with [30]

$$g(x) = \int_0^\infty \frac{y dy}{e^{(y^2 - \mu)/\Theta} + 1} \ln \left| \frac{x+y}{x-y} \right|, \quad (27)$$

and the imaginary part is

$$\omega_i = - \left. \frac{\epsilon_i}{\partial \epsilon_r / \partial \omega} \right|_{\omega=\omega_r}. \quad (28)$$

Noticing that the SDA result has an unphysical cutoff: when k is beyond a certain value, ω_r has no solution and ω_i goes to minus infinity. The simulation results and the AC

numerical results of normal modes match up perfectly. However, the simulation results of high- k modes are not shown, especially in Fig. 7(c), where the damping rates of the simulation points with the largest k are one order lower than the real frequency. We do not present the result of high k because it is found that those high- k modes have uncertain frequency, or, do not damp exponentially, it is impossible to measure the real frequency or the damping rate. The reason for this non-exponential behavior is, as we have mentioned previously, in degenerate plasmas, when k is large enough, the topological shape of the real locus become nonclassical, which results in the frequency and the damping rate of normal modes increase faster than linear with k . Hence, beyond a critical value of k , the normal mode damps faster than the ballistic mode, the time-dependent behavior can then be dominated by the ballistic mode. We surmise that this phenomenon occurs for two reasons: (1) The damping rate increases with k faster in quantum plasmas than in classical plasma, hence the damping rate in quantum plasmas is more likely higher than the normal modes; (2) In our simulation, the initial shape of the perturbation is the same as the equilibrium shape, thus the perturbation possesses a steep edge at the Fermi surface. It is well known that an initial shape with a sharp edge results in ballisticlike time-asymptotic responses [24].

The proof of the above statement is represented in Fig. 8, where the red lines are the pure ballistic evolution obtained by integrate the first term in Eq. (25). In Fig. 8(a), where $\Theta = 0.2$ and $\hbar = 0.6$, when $k = 1.3$, the ballistic mode damps faster than the normal mode, hence the simulation result shows a clear normal mode with $\omega_i = -0.185$ (the dotted line stands for $e^{-0.185t}$). However, when $k = 2.1$, the normal mode should give $\omega_i = -0.944$, while the simulation curve damps slower than $e^{-0.944t}$ and is almost identical to the ballistic mode, and it confirms our conclusion. Also notice that the simulation curve

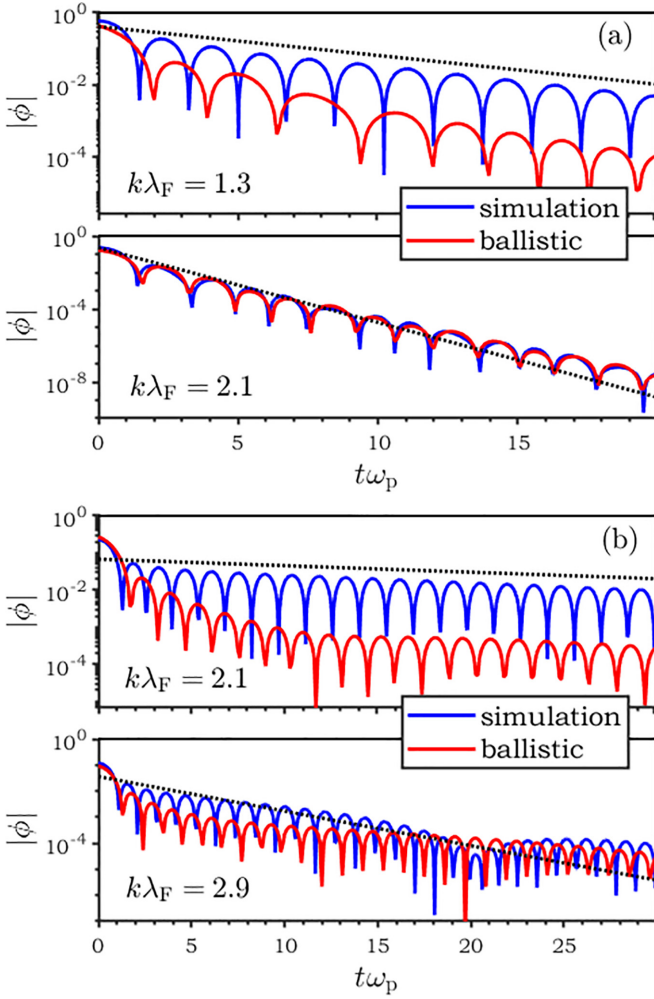


FIG. 8. Temporal evolution of linear perturbations calculated by numerical simulation (the blue lines), and the ballistic evolution (the red lines): (a) $\Theta = 0.2$, $\hat{h} = 0.6$, (b) $\Theta = 0.02$, $\hat{h} = 0.05$. The dotted-lines indicate the damping rate calculated by the eigenequation (14).

does not have a clear real frequency. Similarly, in Fig. 8(b), where $\Theta = 0.02$ and $\hat{h} = 0.05$, a clear normal mode with $\omega_i = -0.0957i$ is measured for $k = 2.1$, but for $k = 2.9$ the long time behavior is interfered by ballistic mode, hence no clear normal mode can be seen.

IV. DISCUSSION AND CONCLUSION

In this paper, we adopt the analytical continuation scheme to solve the dispersion relation of degenerate plasma. Compared to the SDA scheme, the AC scheme can solve

the normal modes of a dielectric system with arbitrarily high k , which is crucial when small-wavelength quantum kinetic effects are encountered. We find that in degenerate plasmas, the normal mode frequency and its damping rate increase with k steeper than linear, which is related to the “quantum” topological shape of the root locus. As a result, the temporal evolution of a high- k perturbation in quantum plasmas is dominated by ballistic mode. Especially, the exact solution of the linear dispersion relation is the basis of the quantitative analysis of nonlinear effects such as parametric decay, two-plasmon decay, Raman scattering, and etc., in dense plasmas.

ACKNOWLEDGMENTS

This work was supported by the Strategic Priority Research Program of Chinese Academy of Sciences (Grant No. XDA250050500), the National Natural Science Foundation of China (Grant No. 12075204), and Shanghai Municipal Science and Technology Key Project (No. 22JC1401500). D.W. thanks the sponsorship from Yangyang Development Fund.

APPENDIX: 1D DIRAC-FERMI DISTRIBUTION FUNCTION

In light of the properties of the polylog functions:

$$\text{Li}_0(z) = \frac{z}{1-z}, \quad (\text{A1})$$

$$\text{Li}_1(z) = -\ln(1-z), \quad (\text{A2})$$

and

$$\frac{d\text{Li}_n(e^x)}{dx} = \text{Li}_{n-1}(e^x), \quad (\text{A3})$$

the 3DFDDF Eq. (3) can be written in the form of

$$f_{3d}(v) = -\frac{3}{4\pi} \text{Li}_0[-e^{(v^2-\mu)/\Theta}]. \quad (\text{A4})$$

Then the 1DFDDF is

$$\begin{aligned} f_{1d}(v_{\parallel}) &= -\frac{3}{2} \int_0^{\infty} \text{Li}_0[-e^{(\mu-v_{\parallel}^2)/\Theta} e^{v_{\perp}^2/\Theta}] v_{\perp} dv_{\perp} \\ &= -\frac{3}{4} \Theta \int_0^{\infty} \text{Li}_0[-e^{(\mu-v_{\parallel}^2)/\Theta} e^{-x}] dx \\ &= -\frac{3}{4} \Theta \text{Li}_1[-e^{(v_{\parallel}^2-\mu)/\Theta}] \\ &= \frac{3}{4} \Theta \ln [e^{(\mu-v_{\parallel}^2)/\Theta} + 1]. \end{aligned} \quad (\text{A5})$$

- [1] D. A. Uzdensky and S. Rightley, Plasma physics of extreme astrophysical environments, *Rep. Prog. Phys.* **77**, 036902 (2014).
 [2] G. Manfredi, P.-A. Hervieux, and J. Hurst, Phase-space modeling of solid-state plasmas: A journey from classical to quantum, *Rev. Mod. Plasma Phys.* **3**, 13 (2019).

- [3] X. Li, D. Xiao, and Z. Zhang, Landau damping of quantum plasmons in metal nanostructures, *New J. Phys.* **15**, 023011 (2013).
 [4] S. H. Glenzer, C. A. Back, K. G. Estabrook, R. Wallace, K. Baker, B. J. MacGowan, B. A. Hammel, R. E. Cid, and J. S. De Groot, Observation of two ion-acoustic waves in a two-species

- laser-produced plasma with Thomson scattering, *Phys. Rev. Lett.* **77**, 1496 (1996).
- [5] J. Zhang, W. M. Wang, X. H. Yang, D. Wu, Y. Y. Ma, J. L. Jiao, Z. Zhang, F. Y. Wu, X. H. Yuan, Y. T. Li *et al.*, Double-cone ignition scheme for inertial confinement fusion, *Philos. Trans. R. Soc. A* **378**, 20200015 (2020).
- [6] A. Bret, F. J. M. Fernández, and J. M. Anfray, Unstable spectrum of a relativistic electron beam interacting with a quantum collisional plasma: Application to the fast ignition scenario, *Plasma Phys. Control. Fusion* **51**, 075011 (2009).
- [7] D. Wu, W. Yu, S. Fritzsche, and X. T. He, Particle-in-cell simulation method for macroscopic degenerate plasmas, *Phys. Rev. E* **102**, 033312 (2020).
- [8] X. Ning, T. Liang, D. Wu, S. Liu, Y. Liu, T. Hu, Z. Sheng, J. Ren, B. Jiang, Y. Zhao *et al.*, Laser-driven proton-boron fusions: Influences of the boron state, *Laser Part. Beams* **2022**, e8 (2022).
- [9] L. D. Landau, On the vibrations of the electronic plasma, *Jetf* **16**, 574 (1946) [*J. Phys. USSR* **10**, 25 (1946)].
- [10] E. M. Lifschitz and L. P. Pitajewski, Physical kinetics, *Textbook of Theoretical Physics* (Elsevier, Oxford, 1983).
- [11] D. Pines and D. Bohm, A collective description of electron interactions: II. collective vs individual particle aspects of the interactions, *Phys. Rev.* **85**, 338 (1952).
- [12] H. Hora, R. Sadighi-Bonabi, E. Yazdani, H. Afarideh, F. Nafari, and M. Ghorannevis, Effect of quantum correction on the acceleration and delayed heating of plasma blocks, *Phys. Rev. E* **85**, 036404 (2012).
- [13] T. Piran, The physics of gamma-ray bursts, *Rev. Mod. Phys.* **76**, 1143 (2005).
- [14] J. J. Brainerd, A plasma instability theory of gamma-ray burst emission, *Astrophys. J.* **538**, 628 (2000).
- [15] J. W. Bates, R. K. Follett, J. G. Shaw, S. P. Obenschain, J. F. Myatt, J. L. Weaver, M. F. Wolford, D. M. Kehne, M. C. Myers, and T. J. Kessler, Suppressing parametric instabilities in direct-drive inertial-confinement-fusion plasmas using broadband laser light, *Phys. Plasmas* **30**, 052703, (2023).
- [16] J.-R. Marquès, C. Briand, F. Amiranoff, S. Depierreux, M. Grech, L. Lancia, F. Pérez, A. Sgattoni, T. Vinci, and C. Riconda, Laser-plasma interaction experiment for solar burst studies, *Phys. Rev. Lett.* **124**, 135001 (2020).
- [17] J. F. Myatt, J. Zhang, J. A. Delettrez, A. V. Maximov, R. W. Short, W. Seka, D. H. Edgell, D. F. DuBois, D. A. Russell, and H. X. Vu, The dynamics of hot-electron heating in direct-drive-implosion experiments caused by two-plasmon-decay instability, *Phys. Plasmas* **19**, 022707 (2012).
- [18] E. Rovere, A. Colaïtis, R. K. Follett, and A. Casner, Hot electron scaling for two-plasmon decay in ICF plasmas, *Phys. Plasmas* **30**, 042104 (2023).
- [19] D. J. Stark, L. Yin, T. B. Nguyen, G. Chen, L. Chacon, B. M. Haines, and L. Green, Nonlinear models for coupling the effects of stimulated raman scattering to inertial confinement fusion codes, *Phys. Plasmas* **30**, 042714 (2023).
- [20] P. Michel, L. Divol, E. L. Dewald, J. L. Milovich, M. Hohenberger, O. S. Jones, L. B. Hopkins, R. L. Berger, W. L. Kruer, and J. D. Moody, Multibeam stimulated raman scattering in inertial confinement fusion conditions, *Phys. Rev. Lett.* **115**, 055003 (2015).
- [21] L. P. Kadanoff, *Quantum Statistical Mechanics* (CRC Press, Boca Raton, FL, 2018).
- [22] T. Dornheim, S. Groth, and M. Bonitz, The uniform electron gas at warm dense matter conditions, *Phys. Rep.* **744**, 1 (2018).
- [23] S. V. Vladimirov and Yu. O. Tyshetskiy, On description of a collisionless quantum plasma, *Phys. Usp.* **54**, 1243 (2011).
- [24] L. Chen, *Waves and Instabilities in Plasmas* (World Scientific, Singapore, 1987).
- [25] J. Lindhard, On the properties of a gas of charged particles, *Kgl. Danske Videnskab. Selskab Mat.-Fys. Medd.* **28**, 8 (1954).
- [26] Q. S. Feng, C. Y. Zheng, Z. J. Liu, L. H. Cao, Q. Wang, C. Z. Xiao, and X. T. He, Stimulated Brillouin scattering behaviors in multi-ion species plasmas in high-temperature and high-density region, *Phys. Plasmas* **26**, 052101 (2019).
- [27] N.-D. Suh, M. R. Feix, and P. Bertrand, Numerical simulation of the quantum Liouville-Poisson system, *J. Comput. Phys.* **94**, 403 (1991).
- [28] F. Haas, B. Eliasson, P. K. Shukla, and G. Manfredi, Phase-space structures in quantum-plasma wave turbulence, *Phys. Rev. E* **78**, 056407 (2008).
- [29] T.-X. Hu, J.-H. Liang, Z.-M. Sheng, and D. Wu, Kinetic investigations of nonlinear electrostatic excitations in quantum plasmas, *Phys. Rev. E* **105**, 065203 (2022).
- [30] C. F. Clauser and N. R. Arista, Stopping power of dense plasmas: The collisional method and limitations of the dielectric formalism, *Phys. Rev. E* **97**, 023202 (2018).